Kinetic Barriers to the Folding of Horse Cytochrome *c* in the Reduced State†

Abani K. Bhuyan* and Rajesh Kumar

School of Chemistry, University of Hyderabad, Hyderabad 500046, India

Received June 28, 2002; Revised Manuscript Received August 22, 2002

ABSTRACT: To determine the kinetic barrier in the folding of horse cytochrome *c*, a CO-liganded derivative of cytochrome *c*, called carbonmonoxycytochrome *c*, has been prepared by exploiting the thermodynamic reversibility of ferrocytochrome *c* unfolding induced by guanidinium hydrochloride (GdnHCl), pH 7. The CO binding properties of unfolded ferrocytochrome *c*, studied by ^{13}C NMR and optical spectroscopy, are remarkably similar to those of native myoglobin and isolated chains of human hemoglobin. Equilibrium unfolding transitions of ferrocytochrome *c* in the presence and the absence of CO observed by both excitation energy transfer from the lone tryptophan to the ferrous heme and far-UV circular dichroism (CD) indicate no accumulation of structural intermediates to a detectable level. Values of thermodynamic parameters obtained by two-state analysis of fluorescence transitions are $\Delta G(H_2O) = 11.65(\pm 1.13)$ kcal mol^{-1} and $C_m = 3.9(\pm 0.1)$ M GdnHCl in the presence of CO, and $\Delta G(H_2O) = 19.3(\pm 0.5)$ kcal mol^{-1} and $C_m = 5.1(\pm 0.1)$ M GdnHCl in the absence of CO, indicating destabilization of ferrocytochrome *c* by ~7.65 kcal mol^{-1} due to CO binding. The native states of ferrocytochrome *c* and carbonmonoxycytochrome *c* are nearly identical in terms of structure and conformation except for the Fe^{2+}−M80 → Fe^{2+}−CO replacement. Folding and unfolding kinetics as a function of GdnHCl, studied by stopped−flow fluorescence, are significantly different for the two proteins. Both refold fast, but carbonmonoxycytochrome *c* refolds 2-fold faster ($\tau = 1092$ μs at 10 °C) than ferrocytochrome *c*. Linear extrapolation of the folding rates to the ordinate of the chevron plot projects this value of τ to 407 μs. The unfolding rate of the former in water, estimated by extrapolation, is faster by more than 10 orders of magnitude. Significant differences are also observed in rate-denaturant gradients in the chevron. Formation and disruption of the Fe^{2+}−M80 coordination contact clearly impose high−energy kinetic barriers to folding and unfolding of ferrocytochrome *c*. The unfolding barrier due to the Fe^{2+}−M80 bond provides sufficient kinetic stability to the native state of ferrocytochrome *c* to perform its physiological function as an electron donor.

Short secondary structural elements in isolation can achieve folding very fast, in nanoseconds to a few microseconds (*1*−*6*). Such a great speed of folding (unfolding), however, is not seen for real proteins. Small single-domain proteins that exhibit two-state kinetics generally fold fast. But there is a considerable variation in the folding rate even among these proteins: some fold with a time constant, τ, in the range ~130−1000 μs (*7*−*13*), while others fold slow, yielding τ of a few milliseconds to tens of milliseconds (*14*−*17*). These observations indicate that the folding speed is set by inherent substantial kinetic barriers so that the rate of folding does not approach the diffusion limit. Further, the kinetic barriers are high for some proteins and low for others, resulting in a wide variation in folding rates.

Kinetic barriers to folding and unfolding could be fortuitous or obligatory. When non-native interactions exist in the unfolded polypeptide ensemble, and if they persist during the folding run, they can retard folding by arresting the partially structured polypeptide into local minima of wrong compact conformations. Folding resumes when the unwanted interaction is ruptured by thermal fluctuations of the molecule. In essence, persistent non-native interactions whose dissolution rates are smaller than the protein-folding rate can act as kinetic barriers. These fortuitous or adventitious barriers (also called "A-type" barrier; ref *18*), can block folding of the entire refolding population or of only a fraction of it, and is exemplified by cis−trans proline isomerization-limited folding-unfolding observed for several proteins (refs *19*−*22*, for example). Obligatory or intrinsic barriers (also called "B-type" barrier; ref *18*), on the other hand, are inherent and purposeful, and hence are evolutionarily conserved. The kinetic barrier imposed by the formation of the set of native-state salt bridges in a hydrophobic interior of the Arc repressor, for example, is an intrinsic barrier even though their replacement by amino acid mutations accelerates the folding rate enormously (*23*).

The folding-unfolding reaction of horse cytochrome *c* presents especially revealing examples of both fortuitous and intrinsic barriers. The unfolded molecules of oxidized cytochrome *c* (ferricytochrome *c*) contain H26 and H33 as the Fe^{3+} coordination ligands (*24*−*27*). Fe^{3+}−H26 and Fe^{3+}−H33 are non-native but stable contacts in unstructured

† This work was supported by the School of Chemistry, University of Hyderabad, and Reddy's Research Foundation, Hyderabad.

* Corresponding author. E-mail: akbsc@uohyd.ernet.in. Fax: 91-40-3012460.

[1] Abbreviations: GdnHCl, guanidinium hydrochloride; CD, circular dichroism; NCO, the native state of carbonmonoxide-bound cytochrome *c*; UCO, the unfolded state of carbonmonoxide-bound cytochrome *c*; MRE, mean residue ellipticity.

10.1021/bi0204443 CCC: $22.00 © 2002 American Chemical Society
Published on Web 09/27/2002

polypeptides, and the dissociation rates of these two ligands from the iron are far smaller than the protein refolding rate (*13*). As a result, during refolding of ferricytochrome *c*, the histidines, along with the polypeptide segments that they belong to, become trapped in the folding structure. This act of misfolding displaces the histidine-resident chain segments from the distal side of the heme to the proximal side of M80. Consequently, folding is retarded because the misconfigured chain organization must spend a long time in a kinetically frozen state before the dissociation of non-native histidines allows ligation of M80 and correct chain configuration. Thus, the dissociation of the non-native histidines at later stages of folding impose a kinetic barrier that is fortuitous, because folding is indeed fast when the polypeptides are allowed to refold under conditions where unfolded-state non-native histidine ligation is abolished (*13*, *18*).

What then is the obligatory barrier for refolding (unfolding) of cytochrome *c*? This is the central theme of the present study. Reduced cytochrome *c* (ferrocytochrome *c*) has been chosen for these experiments because non-native heme ligands do not interfere with inherent accelerated folding of this protein (*13*), and thus there is no fortuitous barrier. A strategic in vitro procedure has been used to replace the $Fe^{2+}-M80$ bond with $Fe^{2+}-CO$ in both native and unfolded states. It is shown that the CO binding properties of GdnHCl−unfolded ferrocytochrome *c* are remarkably similar to those of carbonmonoxymyoglobin, and hence the CO-bound ferrocytochrome *c* is being called carbonmonoxycytochrome *c*, just as the nomenclature carbonmonoxymyoglobin (*28*) and carbonmonoxyhemoglobin (*29*) flows. The replacement suppresses the protein stability from 19.3(±0.5) kcal mol^{-1} to 11.65(±1.13) kcal mol^{-1} at the cost of minimal or virtually no structural alteration. The presence of CO also changes the folding chevron in terms of both the kinetic *m* values and the folding rates in a substantial manner. In the curved folding limbs the refolding time in water scales down from ∼1.99 ms in the absence of CO to ∼1.09 ms in the presence of CO. More dramatic is the effect on the unfolding rate; the $Fe^{2+}-M80 \rightarrow Fe^{2+}-CO$ replacement increases the unfolding rate in water by more than 10 orders of magnitude. The results and analyses demonstrate how the formation and rupture of the $Fe^{2+}-M80$ bond impose obligatory kinetic barriers to in vitro folding and kinetic stability of ferrocytochrome *c*.

MATERIALS AND METHODS

Horse heart cyt *c* (Type VI from Sigma) was used without further purification. GdnHCl and sodium dithionite were obtained from Gibco BRL and Merck, respectively. Protein concentrations were determined by the use of molar extinction coefficients (Table 2). All experiments were done in 0.1 M sodium phosphate buffer in an inert atmosphere. Extreme care was taken to minimize air exposure of solutions. During low-temperature measurements, vapor fogging and condensation on the outer surfaces of cuvettes and flow cells were avoided by blowing a constant stream of nitrogen.

NMR Spectroscopy. A 600 μL solution of unfolded cytochrome *c* (∼2 mM protein, 6.35 M GdnHCl, 0.1 M phosphate, 15% D_2O, pH 6), contained in a 5 mm NMR tube, was deaerated by passing nitrogen into the solution, reduced by the addition of sodium dithionite to a final concentration of 20 mM, and liganded with ^{13}CO by bubbling the gas gently into the solution for ∼30 s. The tube was sealed by the use of a rubber stopper. To ensure complete equilibration, the sealed NMR tubes were shaken gently in dark for ∼30 min. NMR spectra were recorded at 22 °C in Bruker or Varian spectrometers operating at carbon frequencies of 125.7 or 150.9 MHz. The spectra were of 16K data points covering a spectral width of 50 kHz. A relaxation delay of 5 s was employed. Typically, 10 000 scans were averaged.

Equilibrium Unfolding Measurements. Samples of cytochrome *c*, prepared in the 0−8 M range of GdnHCl, contained 10−15 μM protein. The solutions were deaerated and reduced under nitrogen with 0.5−1 mM sodium dithionite and incubated in tightly capped quartz cuvettes or rubber-capped small glass tubes for ∼45 min. Tryptophan fluorescence excited at 280 nm (slit width 0.75 nm) was measured at 358 nm (slit width 1.25 nm) using a 1 cm square quartz cuvette in a photon counting instrument (SPEX 320). Far-UV CD at 222 nm was measured using a 1 mm cylindrical cuvette in a JASCO J720 spectropolarimeter.

For equilibrium unfolding measurement of cyt *c*-CO, the dithionite-reduced samples were saturated with CO by passing a slow stream of the dry gas through the solutions for a minute. To ensure complete equilibration, the sealed tubes were shaken gently in dark for ∼30−240 min at room temperature. Steady incubation of the samples without shaking produced no difference. Fluorescence emission at 358 nm (excitation: 280 nm) was measured at 22 °C using a FluoroMax-3 instrument (Jobin-Yvon, Horiba) setting the excitation and emission slits to 0.75 and 10 nm, respectively. 222-nm CD measurements were performed using rectangular cells (1 mm path length) in a Jasco J715 instrument.

pH Titration of the Unfolded Protein. The pH of an unfolding buffer solution (6.1 M GdnHCl, 75 mM phosphate, 25 mM acetate) was adjusted to different values in the range 7.6−4.6 by the addition of minimal volumes of concentrated phosphoric acid and NaOH. Ten microliters of a 0.14 mM protein solution unfolded in 6 M GdnHCl was added to 1 mL of each of these buffer solutions of variable pH. The samples were then deaerated, reduced under nitrogen by the addition of ∼1 mM sodium dithionite, saturated with CO by passing the gas into the solutions for a minute, and incubated in sealed cuvettes at room temperature in dark for an hour. Optical absorption spectra in the Soret region (475−375 nm) were recorded at 22 °C in a Shimadzu UV-3101PC UV−Vis−NIR spectrophotometer interfaced to a TCC controller.

Measurements of Folding and Unfolding Kinetics. Cytochrome *c* (0.345 mM), initially unfolded in 6.35 M GdnHCl, pH 7, was reduced under nitrogen by the addition of a concentrated solution of sodium dithionite to a final concentration of 3.2 mM and liganded with CO. The CO-saturated unfolded protein solution was loaded in a gastight syringe and equilibrated at 10 °C for ∼10 min. In the meanwhile, the refolding buffer solution containing the desired concentration of GdnHCl was reduced by the addition of dithionite to a final concentration of 3.2 mM and filled in a gastight syringe. The protein and buffer solutions were then loaded into the stopped-flow mixing module that was exhaustively washed with deionized water containing 3.2 mM

sodium dithionite. Folding was initiated by two-syringe mixing: 30 μL of the unfolded protein with 270 μL of the refolding buffer. The total flow rate was 7.143 mL s^{-1}. After recording kinetics at a given concentration of the denaturant, a fresh protein solution and the refolding buffer of another concentration of the denaturant were loaded. This two-syringe procedure ensures minimal air oxidation of the protein. The final protein concentration in the folding mixture was 34 μM. After recording kinetics, the waste solutions were collected to check the GdnHCl concentrations to which the protein refolded and to record visible absorption spectra to ensure that the protein had CO bound to its heme group during the course of measurements.

Unfolding experiments were performed following the same procedure of two-syringe mixing (30 μL of the native protein with 270 μL of the unfolding buffer). The CO-bound native cytochrome *c* was prepared as follows. An unfolded protein solution (~1.3 mM cytochrome *c*, 7.5 M GdnHCl), reduced and liganded with CO, was diluted 5-fold with dithionite-containing native buffer to obtain the CO-bound folded protein in 1.5 M GdnHCl. This procedure was carried out manually in an inert atmosphere at room temperature before loading the protein sample into the stopped-flow syringe. The unfolding buffer containing a desired concentration of GdnHCl was reduced with dithionite, but contained no CO. The final protein concentration in unfolding experiments was ~26 μM. The unfolding kinetics were recorded in less than 5 min of the preparation of the CO-bound native protein.

The kinetics of folding and unfolding were measured using SFM3 or SFM4 mixing modules (Biologic) regulated at 10 °C by the use of an external water bath. The 280 nm excitation source was obtained from a 150 W xenon lamp. Fluorescence emission by the mixed solution, contained in a 0.8 mm square flow cell, was measured at 359 nm. A few refolding traces at lower concentrations of GdnHCl were recorded also by heme optical absorption at 411 and 550 nm. The dead time, determined experimentally by using the procedure suggested by the instrument manufacturer, was ~1.5 ms. Data were acquired using the software provided by Biologic. Typically, 10−20 shots were averaged for noise reduction.

Analysis of Equilibrium Unfolding Curves. The fluorescence data were scaled by dividing the signals at different concentrations of GdnHCl by the signal at the highest concentration of the denaturant. CD data were not subjected to normalization. The observables as a function of GdnHCl were least-squares fitted to a two-state N ↔ U model using eq 1 (*30*):

$$S_{obs} = \frac{C_f + m_f[D] + C_u + m_u[D]\exp\left(\frac{-\Delta G + m_g[D]}{RT}\right)}{1 + \exp\left(\frac{-\Delta G + m_g[D]}{RT}\right)} \quad (1)$$

where S_{obs} is the observed signal, and C_f and C_u and m_f and m_u represent intercepts and slopes of native and unfolded baselines, respectively. m_g (or the equilibrium *m* value) is a parameter related to the change in surface area during the global unfolding of the protein, and [D] represents the concentration of GdnHCl. The far-UV CD signals in the native-state baseline region were fitted to $C_f + m_{f1}[D] + m_{f2}[D]^2$.

Analysis of Kinetic Traces. The time dependence of signals was fitted to single- or double-exponential functions to obtain apparent rates, λ_i, the initial signal, S_0, which corresponds to the "zero-time" signal in the stopped-flow time window, the observed signal, S_{obs}, and the final equilibrium signal, S_∞, corresponding to the signal value at $t = t_\infty$. The S_0, S_{obs}, and S_∞ signals were subjected to initial normalization by first subtracting the buffer fluorescence signals and then dividing by the recorded signal of the unfolded protein in the highest GdnHCl concentration. In the unfolding set of measurements, the S_∞ value of the kinetic trace at the highest concentration of GdnHCl employed was used to divide the fluorescence signals. The GdnHCl dependence of S_0 and S_∞ signals describe the titration of the missing amplitude, which is lost within the dead time of measurement, and the equilibrium global transition, respectively.

Chevron Analysis. The dependence of λ on GdnHCl concentration in the range 1.6−6.5 M was analyzed according to the two-state model, N ↔ U:

$$K = \frac{[U]}{[N]} = \frac{k_u}{k_f}$$

$$\lambda_1 = k_u + k_f$$

$$\log k_u = \log k_u(H_2O) + m_u[\text{GdnHCl}]$$

$$\log k_f = \log k_f(H_2O) + m_f[\text{GdnHCl}] \quad (2)$$

where, $k_u(H_2O)$ and $k_f(H_2O)$ are unfolding and refolding rate constants, respectively, in the absence of GdnHCl.

The denaturant dependence of λ in the entire range of GdnHCl concentration was analyzed by polynomial fits (*31*):

$$\log k_f = \log k_f(H_2O) + m_{1,f}[\text{GdnHCl}] - m_{2,f}[\text{GdnHCl}]^2$$

$$\log k_u = \log k_u(H_2O) + m_{1,u}[\text{GdnHCl}] - m_{2,u}[\text{GdnHCl}]^2 \quad (3)$$

The fitted values of $k_f(H_2O)$ and $k_u(H_2O)$, along with the corresponding *m* values, were compared with those calculated by the use of the equations

$$\log k_f(H_2O) = \log k_u(H_2O) - \log K(H_2O)$$

$$\log k_u(H_2O) = \log k_f(H_2O) + \log K(H_2O) \quad (4)$$

where

$$\log K(H_2O) = -\Delta G(H_2O) + \frac{m_g[\text{GdnHCl}]}{2.3RT}$$

RESULTS

Binding of Carbonmonoxide to Unfolded Ferrocytochrome c. Under normal physiological conditions, the heme group of mitochondrial cytochrome *c* is axially bonded to H18 and M80 and does not bind any other ligand of intra- or extracellular origin. Unfolding of the protein, however, weakens and ruptures the Fe^{2+}−M80 bond and brings about significant changes in heme-ligand chemistry at this axial site (*13*). Advantage can be taken of this fact to engineer

Table 1: ^{13}C Chemical Shifts and Equilibrium Constants for CO Binding to Unfolded Horse Ferrocytochrome *c*, Horse Myoglobin, and Human Hemoglobin[a]

	log K_a (M^{-1})	^{13}C chemical shift (ppm)
horse carbonmonoxycytochrome *c*	7.32	207.91
horse carbonmonoxymyoglobin	7.46(74)	208.29[b,30]
human hemoglobin		
α-chain	8.48(74)	208(31)
β-chain	8.75(74)	207(31)

[a] Conditions, horse ferrocytochrome *c*: 6.35 M GdnHCl, 0.1 M phosphate buffer, pH 6, 20 °C; horse myoglobin, 0.1 M phosphate, pH 7, 20 °C; human hemoglobin, pH 6.35−8, 20 °C. [b] The ^{13}C chemical shift of bound CO in carbonmonoxymyoglobin found in the present study is 209.75 ppm.

the binding of extrinsically added CO. The ^{13}C NMR spectrum of unfolded ferrocytochrome *c* recorded in the presence of saturating amount of ^{13}CO (not shown) confirms CO binding. The resonance at 207.91 ppm (Table 1) is due to the heme-bound ^{13}CO of unfolded carbonmonoxycytochrome *c* (UCO). This chemical shift is very close to reported values of carbon shift of bound ^{13}CO in native hemoproteins: 208.29 ppm for carbonmonoxymyoglobin (*32*), 208 ppm for the α-subunit, and 207 ppm for the *β*-subunit of human hemoglobin (*33*−*35*). In the case of ferrocytochrome *c*, the extent of the ^{13}C shift of the heme-liganded carbonmonoxide depends on the concentration of GdnHCl in the unfolding medium. The protein binds CO even under moderately unfolding conditions, as expected from the mass action principle, but the ^{13}C resonance is shifted upfield by as much as 2 ppm. For example, in the presence of ∼3.5 M GdnHCl, the ^{13}C peak resonates at ∼206.9 ppm (not shown). These chemical shifts are collected in Table 1.

While ^{13}C NMR provides a direct demonstration of CO binding to unfolded ferrocytochrome *c*, the heme optical absorption is the most convenient and useful probe to monitor the conformational changes and kinetic events of folding of carbonmonoxycytochrome *c*. Table 2 presents the relevant changes in the band positions and extinction coefficients of heme absorption in Soret and visible regions caused by CO binding. The Soret band (418 nm; $\pi \rightarrow \pi^*$ transition) of unfolded ferrocytochrome *c* blue-shifts to 414 nm in the presence of CO, indicating ligand binding and the production of a homogeneous population where the sixth axial site of the heme is occupied by CO. In the visible region, CO binding causes both α- and *β*-bands (552.5 and 522 nm, respectively) to broaden and red-shift with a large fall in the extinction coefficient of the α-band.

The heme spectral properties have been used in a number of experiments for the determination of CO binding parameters, including the equilibrium affinity of CO for unfolded ferrocytochrome *c*, the second-order binding rate, and rebinding rate following laser photolysis. The data are not shown. The equilibrium affinity of CO for unfolded ferrocytochrome *c* is of interest in the context of this study (see discussion), and the association constant (K_a, M^{-1}) is given as an entry in Table 1.

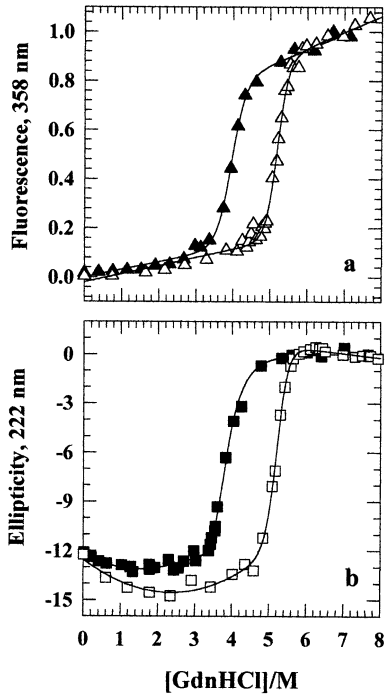

FIGURE 1: GdnHCl-induced equilibrium unfolding of ferrocytochrome *c* in the presence (filled symbols: ▲ and ■) and the absence (open symbols: △ and □) of CO at 10 °C, neutral pH, monitored by (a) tryptophan fluorescence at 358 nm on excitation at 280 nm and (b) far-UV CD. The curves are least-squares fits to the data using a two-state model according to eq 1. The native-state baseline of CD data (b) are approximated by $\theta = c_f + m_1[\text{GdnHCl}] + m_2[\text{GdnHCl}]^2$. Values of ΔG (kcal mol^{-1}) and m_g (kcal mol^{-1} M^{-1}), respectively, obtained are: (a) 11.65(±0.2) kcal mol^{-1} and 2.95(±0.28) kcal mol^{-1}M^{-1} in the presence of CO (▲), and 19.3(±0.5) kcal mol^{-1} and 3.7(±0.2) kcal mol^{-1}M^{-1} in the absence of CO (△); (b) 12.12(±0.7) kcal mol^{-1} and 3.2(±0.1) kcal mol^{-1}M^{-1} in the presence of CO (■), and 20.4(±0.3) kcal mol^{-1} and 3.8(±0.1) kcal mol^{-1}M^{-1} in the absence of CO (□).

Equilibrium Unfolding of Ferrocytochrome c in the Presence of Carbonmonoxide. Because of its preferential binding to the unfolded state of ferrocytochrome *c*, CO is expected to drive the folding-unfolding equilibrium of the protein (N ↔ U; K = U/N) toward the unfolded state. Figure 1a shows the steady-state fluorescence intensity of reduced cytochrome *c* as a function of GdnHCl in the presence and the absence of CO. The unfolding transition curve, indeed, is shifted to the left as a consequence of CO binding to ferrocytochrome *c*. The details of changes in the fluorescence

Table 2: Optical Transitions in Unfolded Ferrocytochrome *c* (6.35 M GdnHCl, 0.1 M Phosphate Buffer, pH 6.5) in the Presence and the Absence of CO (1 atm Pressure)

	λ_{max} (nm)	ϵ (cm^{-1} mM^{-1})	assignment
ferrocytochrome *c*	418	109.74	$\pi \rightarrow \pi^*$ (a_{1u},$a_{2u} \rightarrow e_g$)
(−CO)	522 (*β*)	10.02	$\pi \rightarrow \pi^*$ (vibronic)
	552.5 (α)	13.593	$\pi \rightarrow \pi^*$ (a_{1u},$a_{2u} \rightarrow e_g$)
carbonmonoxycytochrome *c*	414	168.13	$\pi \rightarrow \pi^*$
(+CO)	534	8.69	$\pi \rightarrow \pi^*$
	560	6.28	$\pi \rightarrow \pi^*$

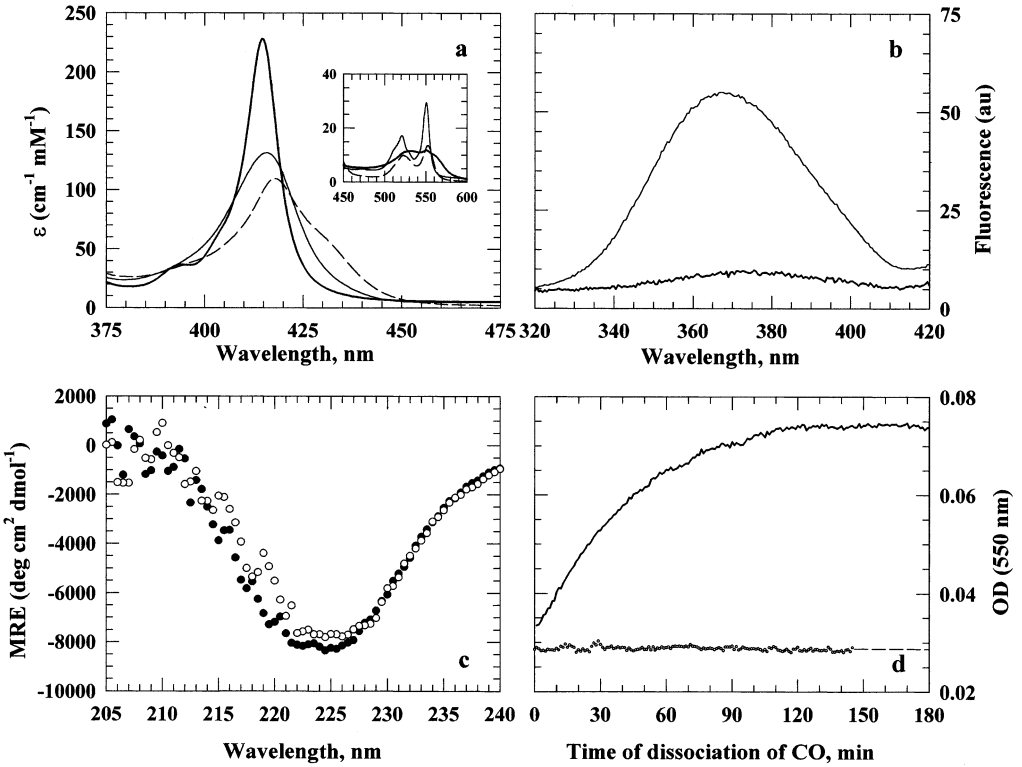

FIGURE 2: Spectral properties and lifetime of native carbonmonoxycytochrome *c*. All measurements on the native proteins were done immediately after their preparation by diluting the unfolded protein solutions. (a) Optical absorption spectra: broken line, $\lambda_{max} = 418$ nm, unfolded ferrocytochrome *c* (6.35 M GdnHCl); continuous line, $\lambda_{max} = 415.5$ nm, native ferrocytochrome *c* prepared by 6.35 → 1.5 M GdnHCl dilution; thick solid line, $\lambda_{max} = 414$ nm, the native state of carbonmonoxycytochrome *c* prepared by 6.35 → 1.5 M GdnHCl dilution of the CO-bound ferrocytochrome *c* solution; the inset shows visible region spectra for these three proteins. (b) Fluorescence spectra of native carbonmonoxycytochrome *c* showing quenched fluorescence emission (thick solid line) obtained by 6.35 → 1.5 M GdnHCl dilution of the unfolded protein solution containing 1 atm CO (thin solid line). (c) Far-UV CD spectra of native states of carbonmonoxycytochrome *c* (●) and ferrocytochrome *c* (○) prepared by 6.35 → 1 M GdnHCl dilution of the corresponding unfolded protein solutions. (d) Kinetics of thermal dissociation of CO from native carbonmonoxycytochrome *c* at 22 °C (thick solid line, $\tau = 40$ min) prepared by 6.35 → 1.5 M GdnHCl dilution of the unfolded protein solution. The flat baseline has been generated by 6.35 → 6.35 M GdnHCl dilution of the unfolded protein solution.

intensity across the unfolding transition and in the post-transition region have been described in detail (*36*, *37*, *13*). In brief, structural unfolding in the transition region produces a sharp increase in tryptophan fluorescence, but the fluorescence continues to increase monotonically in the post-transition baseline region due to a denaturant-dependent continuous expansion of the unfolded chain that results in an increase in the average heme−tryptophan distance. The denaturant dependence of fluorescence values all through the two transitions have been normalized with respect to the fluorescence intensity of completely unfolded proteins (in GdnHCl concentrations of 6.7 and 7.7 M, respectively, in the presence and the absence of CO). The solid lines represent the iterated fits to eq 1. The fit parameters, namely, $\Delta G(H_2O)$, m_g, and C_m ($\cong \Delta G(H_2O)/m_g$), for both transitions are given in the legend to Figure 1.

The GdnHCl-induced unfolding transitions monitored by far-UV CD are shown in Figure 1b. In the presence of CO, the transition has shifted to lower values of the denaturant. Unlike the linear dependence on GdnHCl of fluorescence values in the native baseline region, the CD signals show a pronounced curvature before the onset of sharp signal loss across the global transition regions. This feature has been described previously for ferrocytochrome *c* (*13*), and a second-order polynomial has been used to approximate the native baselines in eq 1. The iterated fit parameters for the two transitions thus obtained are given in the figure legend.

Both probes, tryptophan fluorescence and far-UV CD, yield apparent two-state unfolding transition of ferrocytochrome *c* in the presence of CO. In this paper the value of $\Delta G(H_2O)$ (11.65 ± 1.13 kcal mol^{-1}) obtained from fluorescence will be used to indicate the thermodynamic stability of carbonmonoxycytochrome *c*. $\Delta G(H_2O)$ for ferrocytochrome *c* under identical conditions is 19.3(±0.5) kcal mol^{-1} (see legend to Figure 1).

Preparation and the Identity of Native Carbonmonoxycytochrome c (NCO). Because of the tight affinity of unfolded ferrocytochrome *c* for CO ($K_a = 2.09 \times 10^7$ M^{-1}, Table 1), it is easier to prepare unfolded carbonmonoxycytochrome *c* (UCO), and folding kinetics can be studied simply by diluting the protein with the refolding buffer. Preparation of native carbonmonoxycytochrome *c* (NCO) for unfolding kinetic studies, on the other hand, is not straightforward since the heme iron of native ferrocytochrome *c* does not bind extra-polypeptide ligands. But the refolded product of UCO is NCO, and the latter can be used directly to study unfolding kinetics. It is, of course, necessary to show the spectral and structural properties of NCO and to establish that CO is indeed bound to the refolded product.

Figure 2a shows the Soret heme spectra of NCO, and of native (N) and unfolded (U) ferrocytochrome *c*, all of the same protein concentration (5 ± 0.2 μM). Refolding of ferrocytochrome *c* (U → N) results in a 418 → 415.5 nm blue shift of the Soret peak, accompanied by a loss of the

shoulder. The spectra of N and NCO, both refolded to 1.5 M GdnHCl from the corresponding unfolded states in the presence of 6.35 M GdnHCl, are quite different. The NCO peak (414 nm) is relatively sharp, with an extinction coefficient nearly twice the value for the N peak (415.5 nm). Differences in the visible region are also seen (inset, Figure 2a). These differences mean that refolding of UCO produces the native state of ferrocytochrome *c* with CO still bound to the heme group.

That the CO-bound molecule, refolded from UCO (i.e., UCO → NCO), is structurally and conformationally congruent to native ferrocytochrome *c* can be established from a number of spectroscopic observations. Figure 2b shows fluorescence emission spectra of UCO and NCO, both at identical protein concentration. The UCO molecule is fluorescent (see also Figure 1a), and the emission maximum upon excitation of the tryptophan indole (280 nm) occurs at 367 nm. The NCO emission spectrum shown in Figure 2b was recorded within 2 min of diluting the UCO solution from 6.35 to 1.5 M GdnHCl. In fact, this dilution has been used for preparation of NCO used in the kinetic unfolding studies reported in this work (see below). Since the $Fe^{2+}-CO$ bond is photosensitive, undesirable exposure of the NCO sample to the excitation beam was avoided. The spectrum shown represents just a single emission scan recorded rapidly (5 nm s^{-1}) with minimal opening of the excitation slit. NCO, like native ferrocytochrome *c*, is fluorescence-silent. The quenched fluorescence suggests that in the folded polypeptide of NCO, the center-to-center separation of the heme and the W59 indole is nearly identical to that in native ferrocytochrome *c* (<10 Å; see ref *38*).

Figure 2c shows the peptide CD spectra of NCO and native ferrocytochrome *c* (N) at 22 °C. An unfolded ferrocytochrome *c* solution (6.35 M GdnHCl) was divided into two parts: one was liganded with CO (UCO) and the other was not (U). UCO → NCO and U → N reactions were carried out under identical conditions to a final GdnHCl concentration of 1 M. In each case a two-scan averaged spectrum was recorded within 60 s of refolding. Data below 210 nm were not taken because of large noise in the signal amplified by the presence of slight excess of sodium dithionite that absorbs strongly in this region. The presented spectra show almost identical values of MRE (mean residue ellipticity) for NCO and N. Native ferrocytochrome *c* dissolved directly in 1 M GdnHCl also gives the same spectrum (data not shown). The identical appearance of NCO and N spectra indicates the congruence of the two proteins in terms of secondary structure content. It may be concluded from these results that the NCO species is just the native state of ferrocytochrome *c*, except that CO replaces the M80 ligand.

The NCO protein, even though conformationally equivalent to N, is not stable. The bound CO undergoes slow thermal dissociation to yield to the formation of the $Fe^{2+}-$M80 bond. The reaction $Fe^{2+}-CO \rightarrow Fe^{2+}-M80 + CO$ transforms NCO to N, and this process imposes a time constraint in the use of NCO after its preparation. Figure 2d shows the kinetics of thermal dissociation of CO from NCO at 22 °C. The process can be followed by recording absorbance at 550 nm which is the α-band of visible heme absorption of native ferrocytochrome *c* (inset, Figure 2a). The NCO protein was prepared by 6.35 → 1.5 M GdnHCl dilution of UCO. The baseline signal has been generated by diluting the UCO solution into the unfolding buffer. At 22 °C, ∼10% of the total observable signal is lost by the end of the fifth minute of the measurement. It is thus necessary to minimize the time period between the preparation of NCO and its use in recording unfolding kinetics. Unfolding kinetics reported here were all recorded at 10 °C and within 2−5 min of preparation of NCO. Thus, CO could have dissociated from only a small fraction of NCO molecules (<5%), and the observed unfolding kinetics is almost entirely due to NCO.

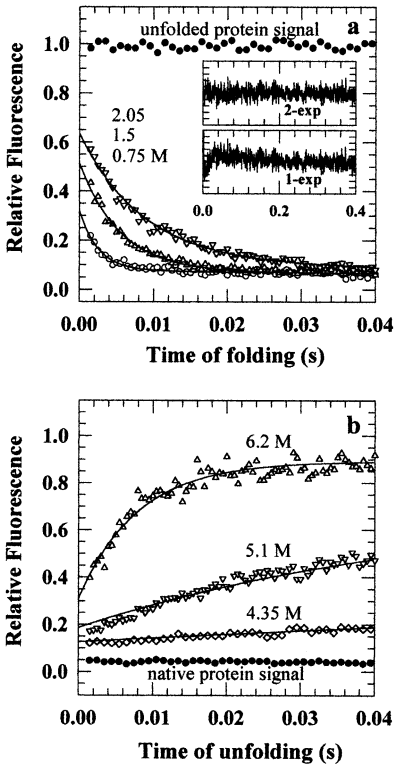

FIGURE 3: Initial 40 ms of fluorescence-monitored stopped-flow kinetic traces at 10 °C, neutral pH. (a) Refolding of carbonmonoxycytochrome *c* is rapid, and a large part of the expected signal with reference to the signal of the unfolded protein (6.1 M GdnHCl, ●) is already lost outside the stopped-flow window; the lower the denaturant concentration in the refolding medium, the larger the loss. The refolding traces are fitted better by a two-exponential function (inset). The major phase is 20−32-fold faster than the minor phase, and the average ratio of the amplitudes of the two phases is 94:6. (b) Observed unfolding kinetics do not indicate submillisecond loss of the expected signal with reference to the fluorescence of the native protein (1.5 M GdnHCl, ●). Unfolding traces are described by a single exponential.

Folding and Unfolding Kinetics of Carbonmonoxycytochrome c. Kinetic Traces. Figure 3a shows the initial 40 ms of a few kinetic folding traces, normalized with reference to the signal of UCO at 10 °C. The folding traces are best described by two exponentials (inset, Figure 3a). In the presence of 0.75 M GdnHCl, the fast phase shows an apparent rate, λ_1, of 400 s^{-1}, and the slow phase decays with λ_2 of 14 s^{-1}. The residuals from single- and double-exponential fits to the data are shown up to 400 ms in the inset to the figure. Relative amplitudes corresponding to the two phases are 0.9 and 0.1, respectively. Refolding to all concentrations of GdnHCl showed two kinetic phases: a fast major phase, and a rather slow minor phase. The amplitude of the minor phase for the refolding runs is no more than

10% of the observed signal, and the averaged relative amplitudes of the two phases are 0.94 and 0.06, respectively.

In the stopped-flow kinetics of refolding of UCO to strongly nativelike conditions, a major fraction of the fluorescence signal expected of the folded protein is already seen to have recovered within the dead time of the instrument (Figure 3a). In the presence of 0.75 M GdnHCl, ~70% of the total expected signal is lost. This lost signal, also called missing amplitude or burst phase amplitude, has a strong dependence on the final concentration of GdnHCl in the refolding milieu; the lower the final denaturant concentration, the larger the missing amplitude (Figure 3a).

Figure 3b shows the initial 40 ms of kinetics of unfolding of NCO in the presence of three concentrations of GdnHCl. The traces have been normalized with respect to the fluorescence signal at $t = t_\infty$ of the unfolding kinetics in the presence of 6.9 M GdnHCl. The entire unfolding course, regardless of the final concentration of the denaturant, fits to a single exponential. Also, the stopped-flow "zero-time signal" does not suggest the occurrence of a significant burst phase reaction. In the presence of 6.2 M GdnHCl, the burst phase accounts for only ~23% of the total expected fluorescence.

Chevron. Figure 4a presents the denaturant dependence of the logarithm of the observed folding and unfolding rates at 10 °C. The transition midpoint, C_m, for the equilibrium N ↔ U transition of ferrocytochrome *c* in the presence of CO is ~3.9 M GdnHCl (Figure 1), which corresponds to the relaxation minimum in the chevron plot (Figure 4a). Expectedly, the apparent rate of folding increases progressively as the GdnHCl concentration in the reaction medium is lowered below the transition midpoint. The folding limb of the chevron is mostly linear. When strongly nativelike conditions are approached (i.e., below ~1.5 M GdnHCl), the folding limb deviates slightly away from the linearity. Similarly, the unfolding rate increases linearly with increasing concentration of the denaturant up to ~6.5 M GdnHCl, beyond which the rate appears to drop slightly.

The apparent rollover of rates under strongly nativelike conditions is not really accentuated. On the basis of the linear functional dependence of protein relaxation rates on the denaturant concentration for most part except for the slight nonlinear regions in the chevron extremities and the correspondence in denaturant concentration of the relaxation minimum and the equilibrium C_m value, a two-state analysis of folding kinetics (NCO ↔ UCO) may be considered. The solid line through the chevron in Figure 4a represents two-state fit of folding kinetics by the use of eqs 2. Rate data in the rollover regions were excluded, and only those in the range 1.5−6.5 M GdnHCl were used to generate the chevron fit (indicated by thick solid line). Values of $k_f(H_2O)$ and $k_u(H_2O)$ obtained from this analysis are listed in Table 3.

Although chevron rollover, in the classical realm of folding kinetics, is generally taken to suggest accumulation of kinetic intermediate (*39*), the phenomenon itself is poorly understood. Factors other than the intrinsically rate-limiting step of a kinetic sequence may also contribute to slowing down the observed rates. Notable is the effect of viscosity of the reaction medium. Concentrated solutions of denaturant are considerably viscous (*40*), and the denaturant viscosity can retard the observed rates, especially in the unfolding limb (*41*). To eliminate the effect of viscosity of GdnHCl solution,

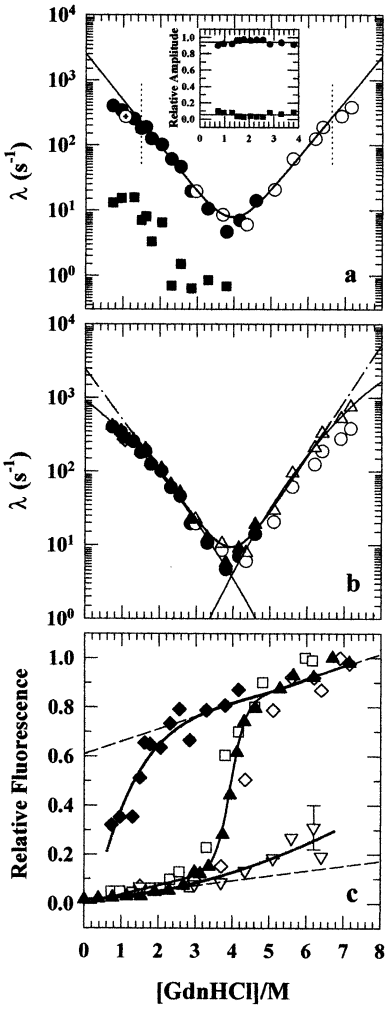

FIGURE 4: (a) Apparent rates of the major phase of folding monitored by fluorescence (●) and Soret heme absorbance at 411 nm (⊕), of unfolding monitored by fluorescence (○), and of the minor phase of folding (■). The boldface line represents two-state fit of the data in the range 1.6−6.4 M GdnHCl (demarcated by vertical dashed lines) by the use of eq 2. The inset shows the 94:6 distribution of amplitudes of the major (●) and the minor (■) phase of folding. (b) The chevron plotted after correction of the apparent rates for the effect of viscosity of GdnHCl: folding rates before and after correction (● and ▲); unfolding rates before and after correction (○ and △). The thick solid line (extrapolated to the ordinate by dash−dot-dash line) is the two-state fit (eq 2) of the corrected chevron using the data in the range 1.6−6.4 M GdnHCl. The thin solid curved lines represent polynomial fit of the viscosity-corrected data by the use of eq 3. (c) Normalized signal values at time $t = 0$ and $t = \infty$ (S_0 and S_∞, respectively) in folding and unfolding kinetics of carbonmonoxycytochrome *c* as a function of GdnHCl: S_0 from refolding (◆) and unfolding (▽), and S_∞ from refolding (□) and unfolding (◇) experiments. The fluorescence-monitored equilibrium unfolding data (▲, see Figure 2a) are also plotted to show that kinetics were recorded long enough for the protein to relax to equilibrium. The solid line through these data represent a two-state equilibrium fit, and yields $\Delta G(H_2O) = 11.75$ kcal mol^{-1} and $m_g = 2.98$ kcal mol^{-1} M^{-1}. Dashed lines represent linear extrapolations of baselines. The area enclosed by S_0 values (◆) under the unfolded baseline extrapolated to the ordinate describes the unobservable amplitudes lost in the dead-time of stopped-flow. The small solid circles (●) through S_0 data represent an empirical fit (see text).

the observed rates can be corrected by using the procedure suggested by Jacob & Schmid (*41*). For clarity the folding chevron is replotted in Figure 4b along with the correction. The correction does alleviate the curvature in Figure 4b,

Table 3: Kinetic Parameters for Folding and Unfolding of Carbonmonoxycytochrome *c* and Ferrocytochrome *c* Obtained from Chevron Analysis as Described in the Text[a]

			$\Delta G(H_2O)$ (kcal mol^{-1})		C_m (M GdnHCl)	
	log $k_f(H_2O)$	log $k_u(H_2O)$	kinetic	equilibrium	kinetic	equilibrium
carbonmonoxycytochrome *c*						
2-state analysis (eq 2)	3.40 (3.39)	−2.14 (−2.34)	7.2 (7.50)	11.65	3.95	3.95
polynomial fit (eqs 3 and 4)	2.96 (2.96)	−4.30 (−4.34)	9.7 (9.75)	11.65	3.95	3.95
ferrocytochrome *c* (eqs 3 and 4)[b]	2.7	−15.3 (−15.2)	23.2	19.3	4.95	5.1

[a] Values within brackets are obtained after correcting the observed rates according to log λ_{corr} = log λ_{obs} + log(η/η_o), where η and η_o are viscosities in the presence and the absence, respectively, of GdnHCl. [b] Data from ref *13*.

especially in the unfolding limb, although not entirely. Two-state values of $k_f(H_2O)$, $k_u(H_2O)$, and $\Delta G(H_2O)$ (eq 2) obtained for the corrected chevron are given in Table 3. The value of 7.5 kcal mol^{-1} for $\Delta G(H_2O)$ determined from this analysis is less than that obtained from equilibrium unfolding data by 4.15 kcal mol^{-1} (Table 3, Figure 1a).

Figure 4b also shows the two-state analysis taking the chevron curvature into account. The analysis is based on a second-order polynomial functional dependence of the rates on the denaturant (equations 3,4; ref *31*). The polynomial-fitted values of $k_f(H_2O)$ and $k_u(H_2O)$ are listed in Table 3. The value of 9.7 kcal mol^{-1} for $\Delta G(H_2O)$ calculated in this way compares with 11.65 kcal mol^{-1} obtained from equilibrium unfolding data (Table 3, Figure 1a). Given the noise in data and the long extrapolation of the unfolding limb to the ordinate, the significance of this difference of 1.95 kcal mol^{-1} in the values of $\Delta G(H_2O)$ cannot be stressed.

Signal Amplitudes. Figure 4c presents a quantitative picture of denaturant dependence of fluorescence signal amplitudes at times $t = 0$ and $t = \infty$ of folding and unfolding kinetics. The fluorescence signal at both $t = 0$ and $t = \infty$ of folding kinetics (S_o^{fol} and S_∞^{fol}, respectively) have been normalized with reference to the fluorescence of the initial unfolded protein. Similarly, S_o^{unfol} and S_∞^{unfol} are, respectively, $t = 0$ and $t = \infty$ fluorescence of unfolding kinetics normalized with respect to the $t = \infty$ signal of unfolding in the presence of the highest concentration of GdnHCl employed. The denaturant dependence of both sets of values, S_∞^{fol} and S_∞^{unfol}, coincide, within experimental error, with the equilibrium unfolding transition, NCO ↔ UCO (Figure 4c), indicating that kinetics were recorded long enough for the protein to relax to equilibrium. The solid line through these $S_\infty^{fol,unfol}$ data points has been drawn using the equilibrium unfolding parameters given in the legend to Figure 1a. The value of S_o^{fol} decreases as the concentration of GdnHCl in the folding medium falls, consistent with the observations made in Figure 3a. The area between the S_o^{fol} values and the unfolded baseline extrapolated linearly to nativelike conditions contains the unobservable fluorescence signal associated with burst phase folding kinetics. The GdnHCl dependence of the S_o^{fol} values may, in principle, be used to describe the melting transition of the product of the burst phase reaction. There is some scatter in the S_o^{fol} data, and their GdnHCl dependence does not indicate a distinct denaturant-induced phase transition. The data in the range 0.6−6.0 M GdnHCl simulate the empirical relation, $S_o = a + bx + cx(\exp(-dx))$, where *a*, *b*, *c*, and *d* are constants and *x* is the concentration of GdnHCl. The denaturant distribution of S_o^{unfol} (Figure 4c) shows that only a minor fraction of the total expected unfolding amplitude is lost in the bursts phase. With the available data, it is difficult to determine whether the S_o^{unfol} values define a simple linear extension of the native-state baseline into the unfolding region or an unfolding process faster than measurable by stopped flow.

Ligand-Based Homogeneity of the UCO Population. The heme-ligand chemistry plays an important role in the folding of cytochrome *c* (*13*), and it is important to establish the nature of unfolded-state heme ligation after the addition of CO. Unfolding of ferrocytochrome *c* at neutral pH results in the rupture of the Fe^{2+}−M80 bond, and the heme site exhibits a dynamic intrapolypeptide ligand equilibrium involving H26, H33, M65, and M80. CO, by virtue of its tight binding to the unfolded-state heme iron, is expected to replace all non-native ligands to yield a ligand-based homogeneous population of UCO. To check if this indeed is true so that the possibility of interference of folding with non-native intrapolypeptide ligand could be excluded altogether, a few relevant equilibrium heme absorption spectra of UCO are examined in Figure 5. The objective is to show a complete displacement of all kinds of ligands by CO.

Displacement of Methionine and Histidine by CO. The unfolded-state heme-ligand equilibria of ferrocytochrome *c* can be modulated to a large extent by the addition of excess of extrinsic histidine and methionine, preferably, their analogues, and the resultant changes are easily detected by shifts in both the band position and the extinction coefficient in the Soret region of the heme absorption spectrum. Figure 5a shows that the unfolded-state spectrum of ferrocytochrome *c* in the presence of 200-fold molar excess of NAM (*N*-acetyl-DL-methionine), a water-soluble analogue of methionine, changes dramatically when 1 atm of CO is added, indicating the ability of CO to displace this ligand completely. Similar experiments show that CO readily displaces the imidazole ligand bound to the Fe^{2+} iron (not shown). These results suggest that the UCO population consist only of CO-bound hexacoordinate molecules.

pH Dependence of Soret Spectra of UCO. To show further that the UCO population is homogeneous and that the CO ligand is irreplaceable by the intrapolypeptide histidines, H26 and H33, the Soret spectrum of UCO can be examined in the pH range through the pK_a of imidazole ionization. Protonation of the imidazole side chain results in deligation, and hence a change in the Soret spectrum. Figure 5b shows that the Soret spectrum of UCO (in 6 M GdnHCl) at different values of pH in the range 7.6−4.6 changes little. The peak absorption maximum stays constant (414.1 ± 0.1 nm). A slight variation in the peak intensity is due to differences in protein concentration. Clearly, the possibility of non-native histidine ligation in the unfolded molecules in the presence of CO is precluded. These are strong indications that the

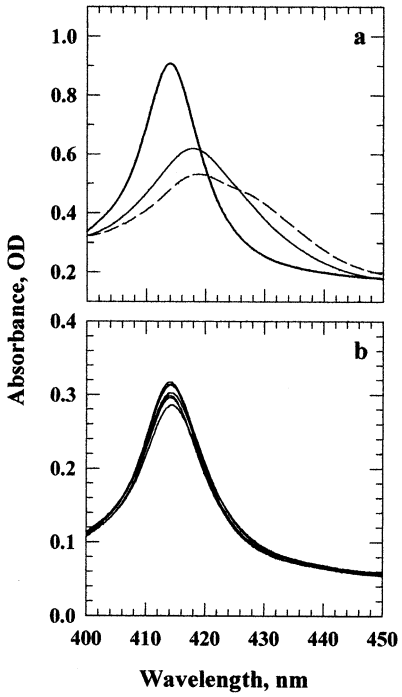

FIGURE 5: (a) Soret spectra showing the replacement of ligands from the heme iron of the unfolded protein: broken line, unfolded ferrocytochrome *c* (6.35 M GdnHCl, pH 7, 22 °C); thin solid line, the same unfolded protein in the presence of 200-fold molar excess of NAM (*N*-acetyl-DL-methionine); thick solid line, when CO is added to the NAM-containing protein solution. (b) Soret spectra of carbonmonoxycytochrome *c* in the pH range 7.6−4.6 in the presence of 6 M GdnHCl, 24 °C. The λ_{max} is a constant (414.1 ± 0.1 nm).

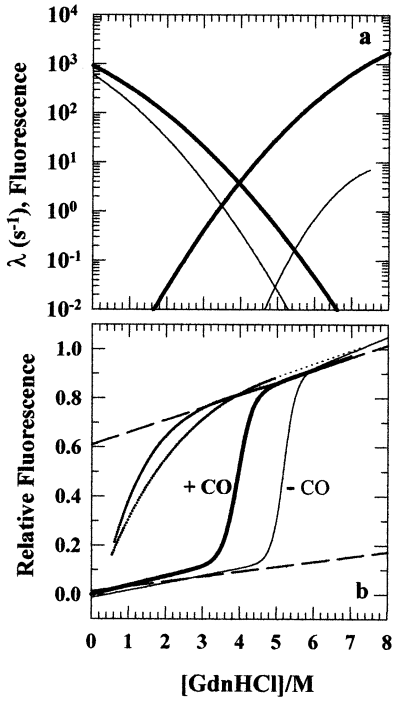

FIGURE 6: Comparison of the denaturant dependence of rates and amplitudes between ferrocytochrome *c* (thin lines) and carbonmonoxycytochrome *c* (boldface lines) studied under identical conditions. (a) Two-state polynomial fits (eq 3) of folding chevrons. Note the vertical and horizontal shifts of the carbonmonoxycytochrome *c* chevron relative to that of ferrocytochrome *c*. (b) GdnHCl dependence of S_0 and S_∞ signals. The S_∞ signals reproduce the respective equilibrium unfolding transitions, and the denaturation midpoints, C_m, match the inflection points in the chevrons. The denaturant distribution of S_0 values are similar for both the proteins, and they do not indicate, within the error limit, the titration of a submillisecond species. The data for ferrocytochrome *c* have been taken from ref *13*.

UCO population is homogeneous in terms of heme−CO ligation.

Comparison of Denaturant Dependence of Folding−Unfolding of Ferrocytochrome c and Carbonmonoxycytochrome c: The Salient Points. Figure 6a illustrates the effect of Fe^{2+}−M80 → Fe^{2+}−CO replacement on the folding chevron obtained under identical experimental conditions. Clearly, both folding and unfolding rates of carbonmonoxycytochrome *c* are larger at all concentrations of GdnHCl. The relative increase in the unfolding rates is more substantial. The polynomial-fitted values of $k_f(H_2O)$, $k_u(H_2O)$, and $\Delta G(H_2O)$ according to eqs 3 and 4 are given in Table 3. The rate-denaturant gradients of both chevrons change continuously, but the gradient becomes relatively shallower for carbonmonoxycytochrome *c* as the denaturant concentration in the medium falls. As the ordinate intercepts indicate, the refolding rate of carbonmonoxycytochrome *c* is just 2-fold larger than that for ferrocytochrome *c*, but the unfolding rate is larger by more than 10 orders of magnitude (Table 3). Figure 6b compares the GdnHCl dependence of S_o^{fol}. The distributions are very similar, suggesting that the immediate response of the unfolded polypeptides on being driven to fold is similar for ferrocytochrome *c* and carbonmonoxycytochrome *c*.

DISCUSSION

Carbonmonoxycytochrome c: The Identity. Cytochrome *c* acts as both an electron-transfer protein in the mitochondrial respiratory chain and a proapoptotic protein in the genetically destined cell death program, and for neither of these functions does it require binding of CO. The iron atom of the protoporphyrin IX heme prosthetic group of cytochrome *c* forms two out-of-plane coordinate bonds with the polypeptide chain: one with the sulfur of M80 and another with the imidazole side chain of H18. The resulting hexacoordinate structure of the heme iron along with the native tertiary fold of the polypeptide around it precludes binding of non-native ligands. Extrinsically added cyanide (CN) and imidazole (Im), nonetheless, form Fe^{3+}−CN and Fe^{3+}−Im bonds by displacing the M80 sulfur in ferricytochrome *c* even under physiological conditions (*42*). But the situation reverses dramatically when ferricytochrome *c* is converted to ferrocytochrome *c* by merely reducing the Fe^{3+} atom to Fe^{2+}. The Fe^{2+}−M80 bond in native ferrocytochrome *c* is so strong that even CO fails to rupture it (*43*). The preparation of the CO derivative of ferrocytochrome *c* is, however, needed for a number of studies related to protein function, motion, and ligand binding dynamics. For such studies, CO ligation has hitherto been achieved by allowing the ligand to bind to the ferrous form of the chemically modified protein in which the M80 sulfur is carboxymethylated in order to prevent its coordination with the iron (*42*, *44*−*48*). It has also been known for half of a century that CO complex of ferrocytochrome *c* can be formed at extremely alkaline pH values (*49*, *44*).

The present work shows how denaturant-induced unfolding of ferrocytochrome *c* facilitates the protein−CO reaction.

This approach was necessary to achieve the objective of finding out the kinetic barrier. The rationale and the mechanism of the denaturation-coupled CO ligation process are simple. In unfolded ferrocytochrome *c* at neutral pH the Fe^{2+}−H18 bond stays intact, but the Fe^{2+}−M80 bond is ruptured, an indication of which is obtained by examining the pure chemical exchange cross-peaks in a 2D exchange NMR spectrum recorded on a sample poised at the midpoint of the equilibrium unfolding transition (unpublished result). The sixth coordination site, as a result of departure of M80, becomes available for potential intrachain heme ligands, namely H26, H33, M65, and M80. Indeed, all four serve as the sixth coordination ligand of the ferrous heme iron in the form of transient contacts (*50*, *13*). When CO is added to the unfolded protein solution, the transient intrachain ligands are effectively replaced by CO, for thermodynamic rather than kinetic reasons (see below). The resultant ensemble of the unfolded protein is now homogeneous in regard to the presence of the Fe^{2+}−CO bond (see below; also Figure 5). The CO-liganded derivative is like a chemically engineered mutant and can be treated as an independent and "self-sufficient" system to study several important aspects of folding−unfolding and motional dynamics of ferrocytochrome *c*. It can be refolded and unfolded, akin to a double-jump experiment, to examine the limiting role of the Fe^{2+}−M80 contact in folding.

A question concerning the number of CO molecules bound per molecule of ferrocytochrome *c* arises. Because NMR exchange spectra across the unfolding equilibrium of ferrocytochrome *c* provide direct evidence for rupture of the Fe^{2+}−M80 bond in the unfolded state, binding of one CO molecule on the M80 side of the heme is easily envisioned. But in view of a substantially large binding constant of CO to the unfolded heme (Table 1), binding of another CO on the H18 side of the heme due possibly to weakening of the Fe^{2+}−H18 bond is not precluded. Further studies will be needed to address this issue.

Apparent Two-State Equilibrium Unfolding of Carbonmonoxycytochrome c. Both probes, tryptophan fluorescence and far-UV CD (Figure 1), indicate that the equilibrium unfolding of ferrocytochrome *c* in the presence of CO involves only the native and the unfolded state without accumulation of structural intermediates to any detectable level. Apparent two-state nature of unfolding is seen in the absence of CO as well (Figure 1), consistent with earlier reports (*13*, *50*), suggesting that CO binding does not stabilize any possible structural intermediate. The presence of structural species intermediate between the native and the unfolded state of ferrocytochrome *c* in the presence or the absence of CO cannot, however, be precluded from these observations. Intermediates of transient lifetime escape detection in conventional equilibrium experiments. It is known that the GdnHCl-induced N ↔ U equilibrium of ferrocytochrome *c* involves at least one short-lived partially unfolded state identifiable by stopped-flow NMR hydrogen exchange measurements under moderate to strongly destabilizing conditions (*51*). Subsequent native-state hydrogen exchange (HX) studies have shown the existence of two more short-lived intermediate structures (*52*). These observations on ferrocytochrome *c* raise important questions concerning the existence, the identity, and the enumeration of transient intermediate structures involved in the folding-unfolding equilibrium of carbonmonoxycytochrome *c*. Strategic HX experiments will be needed to obtain a detailed picture of the equilibrium.

Stability of Carbonmonoxycytochrome c. The unfolding free energy, $\Delta G(H_2O)$, of ferrocytochrome *c* is 19.3(±0.5) kcal mol^{-1} (Figure 1, Table 3), consistent with previous reports (*13*, *53*). The C_m value associated with the transition is 5.1 ± 0.15 M GdnHCl at 10 °C (Table 3). Indeed, ferrocytochrome *c* is one of the most stable proteins known to date. But the value of $\Delta G(H_2O)$ for carbonmonoxycytochrome *c* is 11.65 ± 1.13 kcal mol^{-1} (Figure 1). The difference of 7.65 kcal mol^{-1} ($\Delta\Delta G(H_2O)$) in the free energy of folding between ferrocytochrome *c* and carbonmonoxycytochrome *c* indicates a drastic destabilization of the protein caused by CO binding. The stability loss may appear to reflect destabilization of the native protein consequent upon disruption of the Fe^{2+}−M80 bond by CO. But the destabilization is also associated with a change in m_g, the equilibrium *m* value; it changes from 3.7 ± 0.4 to 2.95 ± 0.28 kcal mol^{-1} M^{-1}. The decrease may be due to increased population of structural intermediates (*53*) as well as because of a more compact denatured state (*54*, *55*). The Fe^{2+}−M80 → Fe^{2+}−CO replacement could be similar to the weakening of the Fe^{2+}−M80 bond in oxidized cytochrome *c* where equilibrium intermediates unobservable in optically monitored unfolding have been shown to be present (*53*). The decrease in m_g also indicates that part of the stability loss of ferrocytochrome *c* due to CO binding is a consequence of the altered structure of the unfolded state.

The alterations in the structure of unfolded ferrocytochrome *c* caused by CO binding can be understood by considering the following scheme depicting the dynamics of unfolded-state heme−protein interactions reported in previous studies (*13*, *50*) (Scheme 1).

Scheme 1

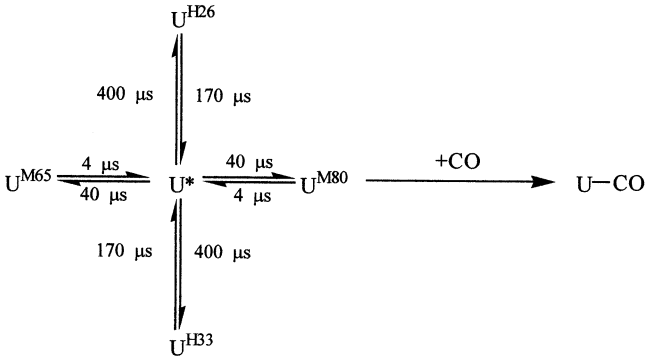

U* represents the five-coordinate form, and superscripts to U identify the residues that serve as intrapolypeptide ligands of the heme iron atom. The consequences of the CO binding reaction are (1) a decrease in enthalpy due to preferential U−CO bonding and (2) an increase in chain configurational entropy due to removal of the loops in the chain ensemble. The four loops existing before CO binding are formed of chain segments H18-M80, H18-M65, H18−H33, and H18−H26, all mediated by bonding of the terminal residues of the segments with the Fe^{2+} atom. The loops, taken as intrachain links, could serve to constrain the number of

conformations accessible to the unfolded chain and that would lower the configurational entropy. In the absence of the intrachain loops, the unfolded state is expected to be more stable. The stabilization energy, estimated from the equilibrium association constant of CO with the unfolded protein (log $K_a \approx 7.32$; Table 1), is ~9.7 kcal mol^{-1}.

Now, the ΔG values available for three branches of the following thermodynamic cycle (Scheme 2)

Scheme 2

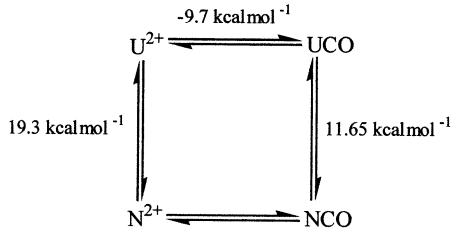

yield ~2 kcal mol^{-1} for the free energy corresponding to the destabilization of the native state of ferrocytochrome *c* by CO binding. We note that the free energy associated with the $Fe^{2+}-M80$ bond is only of this order (*56*). This observation demonstrates that the predominant cause of the decreased stability of carbonmonoxycytochrome *c* is stabilization of the denatured state.

The thermodynamic affinity of the unfolded protein for CO can be thought of as to how much of the intrinsic energy of the $Fe^{2+}-CO$ bond is spent to change the chain configuration. The bond energy, more or less, is used to break the intrachain loops that leads to the expansion of the polypeptide chain. On the basis of these considerations along with various ΔG values found here Figure 7 shows a free energy diagram depicting the effect of CO binding on the stability of native and unfolded states of ferrocytochrome *c*. The energy levels are also consistent with kinetic data (see below).

Rapidity of Folding and Unfolding of Carbonmonoxycytochrome c. Within the limit of stopped-flow resolution (dead-time ≈ 1.5 ms), ~94% unfolded molecules of carbonmonoxycytochrome *c* refold extremely fast. The remaining 6% molecules (see Figure 4a) represent most likely the fraction of oxidized protein that does not bind CO or a small population of nonmonomeric aggregated product. This minor population refolds ~32-fold slower when nativelike conditions (<1 M GdnHCl) are approached. For the fast-folding molecules the rate constant, $k_f(H_2O)$, is 2455 s^{-1} ($\tau \approx 407$ μs, Table 3), when estimated from the two-state analysis of rate-denaturant data in the GdnHCl concentration range 1.5−6.5 M (equation 2), but decreases to 915 s^{-1} ($\tau \approx 1092$ μs) when the entire rate-denaturant space is analyzed by the use of eq 3 to account for the chevron curvature (see Figure 4, Table 3). We must note the deficiencies in our general understanding, analysis, and interpretation of curvatures in protein folding chevrons. To make progress in the present situation, the folding time constant of carbonmonoxycytochrome *c* measured by tryptophan fluorescence at 10 °C is projected in the range 407−1092 μs (Figure 4a,b).

Submillisecond folding rapidity has recently been shown for a few monomeric proteins, including the N-terminal domain of λ repressor (3600 ± 400 s^{-1} at 37 °C; ref *7*) and cold shock proteins CspB (1070 ± 20 s^{-1} at 25 °C; ref *8*)

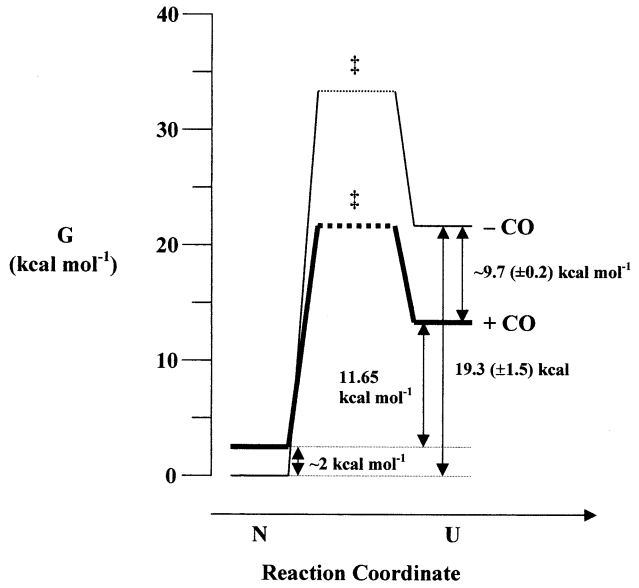

FIGURE 7: Diagram illustrating the effect of $Fe^{2+}-M80 \rightarrow Fe^{2+}-CO$ replacement on the relative free energies of native and unfolded states and the intervening activation barrier(s) in cytochrome *c*. The energy levels were estimated from kinetic parameters that describe the folding chevrons (Figure 6, Table 3), thermodynamic parameters derived from equilibrium unfolding experiments (Figure 1a, Tables 3), equilibrium constant for the association of CO with unfolded ferrocytochrome *c* (Table 1), and temperature dependence of refolding rates of ferrocytochrome *c* in the presence of 1.1 M GdnHCl (data not shown). Due to this synthesis from several lines of evidence, the energy levels of transition states may not appear scaled exactly as described in the text. The error falls in the range 0.3−2 kcal mol^{-1}. The free energy of the native state of ferrocytochrome *c* is arbitrarily set to zero.

and Bc-Csp (1370 ± 140 s^{-1} at 25 °C; ref *11*). It will be useful to examine these rates normalized with reference to the temperature. Generally, a reaction with an activation energy of 12 kcal mol^{-1} is expected to speed up by a factor of 2 for every 10 K rise in temperature. Indeed, the activation energy for refolding of ferrocytochrome *c* in the presence of 1.1 M GdnHCl obtained from Eyring analysis of the temperature dependence of folding rates is ≈12 kcal mol^{-1} (unpublished result). Assuming that the general rate-temperature relation holds for protein folding reaction as well, especially within the small range of temperature relevant here, the value of $k_f(H_2O)$ for carbonmonoxycytochrome *c* will scale-up to the range 2745−7575 s^{-1} ($\tau \approx 158-437$ μs) at 25 °C. This is extremely rapid folding, perhaps next only to the folding of the C-terminal domain of the prion protein (*12*).

Carbonmonoxycytochrome *c* unfolds also rather fast in a single observable phase. The unfolding rate constant in water, $k_u(H_2O)$, projected from chevron analyses by the use of eqs 3, is in the range $3 \times 10^{-3}-4.6 \times 10^{-5}$ s^{-1} ($\tau = 334-2174$ s) at 10 °C (Figure 4, Table 3). Application of the rate-temperature relation casts a value in the range $9 \times 10^{-3}-1.4 \times 10^{-4}$ s^{-1} ($\tau = 111-714$ s) at 25 °C, far smaller than the $k_u(H_2O)$ value of ~10 s^{-1} at 25 °C reported for the unfolding of CspB (*8*). The unfolding rates of carbonmonoxycytochrome *c* in higher concentrations of GdnHCl are, however, unusually fast (Figure 4). For example, when the unfolding milieu contains 6.9 M GdnHCl, the rate is 279 s^{-1} (526 s^{-1}, after correction for the viscosity effect of the denaturant). Further studies of this unfolding reaction will

provide much sought information regarding the fast events in protein unfolding.

Two-State or Multi-State Kinetics? Of the four standard criteria for apparent two-state folding kinetics, namely, (i) both folding and unfolding reactions must display monophasic kinetics (allowing for minor heterogeneity of the unfolded state), (ii) the denaturant concentration corresponding to the bottom of the chevron must match the equilibrium C_m value, (iii) the denaturant dependence of folding and unfolding rates must be linear, and (iv) values of $\Delta G(H_2O)$ and m calculated from kinetic data must match those determined from two-state analysis of equilibrium unfolding data, only the first two stand strictly the test for two-state folding-unfolding kinetics of carbonmonoxycytochrome *c* in the classical sense. The value of $\Delta G(H_2O)$ obtained from polynomial analysis (eq 3) of the chevron is fairly close to the one from the equilibrium transition, but the value derived from two-state analysis (eq 2) is smaller by ~4 kcal mol^{-1} (Table 3). Such a discrepancy in the value of $\Delta G(H_2O)$ obtained from equilibrium and kinetic analyses, observed here as well as in a previous study of the folding of ferrocytochrome *c* (Table 3, and ref *13*), arises mainly from the long extrapolation employed to estimate $k_f(H_2O)$ and $k_u(H_2O)$. Given this the available data and their interpretations are not sufficient to make a case for or against the involvement of intermediate structures. But considering the apparent two-state kinetics of ferrocytochrome *c* under identical conditions (*13*) (see also Figure 6), it is likely that no kinetic intermediate of carbonmonoxycytochrome *c* accumulates.

Burst Phase Of Folding. In folding kinetics of carbonmonoxycytochrome *c*, a part of the total expected fluorescence signal is already lost in the submillisecond time−the stronger the refolding condition, the larger the signal loss. In the presence of 0.75 M GdnHCl, ~70% of the total fluorescence signal is immeasurable in the stopped-flow window (Figure 3a). Certainly, some kind of fast chain reorganization event(s) that results in quenching of tryptophan fluorescence occurs in the stopped-flow dead time. The origin of folding burst signals, whether from a specific and productive chain collapse or from a mere nonspecific chain contraction on being driven from a strongly unfolding to a strongly refolding solvent, remains uncertain. Evidence has been presented in the literature to support both interpretations for the burst phase in the folding kinetics of ferricytochrome *c* (*57*−*64*). It is also possible that burst kinetics entail the presence of a sequence of polypeptide-contracted states, akin to a higher-order continuous transition, that can increasingly restrict the conformational search. With the limited data available in the present study we abstain from commenting further on the origin of the burst signal.

Folding-Unfolding of Carbonmonoxycytochrome c and Ferrocytochrome c. As has been detailed above, carbonmonoxycytochrome *c* is prepared from ferrocytochorme *c* by replacing the iron−M80 ligand with a CO molecule. The change destabilizes ferrocytochrome *c* substantially ($\Delta\Delta G(H_2O) = 7.65$ kcal mol^{-1}; Figure 1, Table 3), but the structures of the two proteins are nearly identical. The subtle perturbation also produces a dramatic change in folding−unfolding kinetics under identical experimental conditions (Figure 6, Table 3).

Both folding and unfolding rates of carbonmonoxycytochrome *c* are faster than those for ferrocytochrome *c*. By assuming that the apparent activation energies for folding and unfolding in water, E_a^f and E_a^u, respectively, are given by an expression of the type $E_a = -RT \ln(k/A_o)$, where k is the rate constant ($k_f(H_2O)$ and $k_u(H_2O)$) and A_o is the preexponential factor, the heights of the activation barriers for folding and unfolding in water can be estimated for both the proteins. The factor A_o can be set to $\sim 2 \times 10^{10}$s^{-1}. This value has actually been determined in refolding experiments of ferrocytochrome *c* in the presence of 1.1 M GdnHCl (unpublished result). The magnitudes of $k_f(H_2O)$ and $k_u(H_2O)$ (Figure 6 and Table 3) show that E_a^f and E_a^u for carbonmonoxycytochrome *c*, relative to ferrocytochrome *c*, are smaller by ~0.4 and ~14.2 kcal mol^{-1}, respectively (Figure 7). The transition-state energy levels in the figure may not appear scaled exactly to yield these values because of errors (0.3−2 kcal mol^{-1}) in the evaluation of the ground-state energy. The scenario, is however, consistent with faster folding and unfolding of carbonmonoxycytochrome *c* and, together with observed equilibrium stabilities (Figure 1), properties of unfolded states (Figure 5), and chevron features (Figures 4,6), provides a framework to understand how cytochrome *c* folds.

Kinetic Mechanism of Cytochrome c Folding. Refolding. Heme-ligand exchange reactions in the unfolded polypeptide play a key role in the folding of cytochrome *c* (*13*, *18*, *24*−*27*, *60*, *65*). A model of heme-ligand exchange dynamics proposed recently explains how ligands can arrest and retard folding of ferricytochrome *c* but not interfere with the folding of ferrocytochrome *c* (*13*). Scheme 1 shows the essential parts of the model relevant for the present. It can be shown, by using the microscopic rates of the four equilibria, that the ratio of equilibrium populations of unliganded (U*, five-coordinate form) and liganded (U^i, where i is the intrapolypeptide ligand) molecules in the unfolded ensemble of ferrocytochrome *c* is 45:55. The U* molecules, which have no equilibrium occupancy at the sixth coordination site of the heme, will fold unaffected. In the case of the U^i molecules, a liganded form will enter the folding pathway only if the rate of dissociation of the ligand from the heme iron is slower than the folding rate (see ref *66*). The dissociation times for all four ligands of ferrocytochrome *c*, as Scheme 1 shows, are smaller than the refolding time of the polypeptide ($\tau \sim 1.99$ ms). We note that this value of τ for refolding of ferrocytochrome *c*, obtained strictly from the curved chevron (Figure 6), allows for the maximum upper limit. The folding chevron of ferrocytochrome *c* is linear when kinetics are measured by Soret heme absorbance. On the basis of this fact, backed by extensive model calculations, the refolding time of ferrocytochrome *c* at 10 °C has been set at 370 ± 180 μs (*13*). In any case, ligand dissociation times would be smaller than the refolding time. Consequently, heme ligation in the unfolded state of ferrocytochrome *c* does not interfere with refolding.

Now, the present study shows that when the intrapolypeptide−heme ligation is abolished by the addition of CO the value of τ decreases from 1.99 to 1.09 ms (Figures 4 and 6). This observation suggests that even though the non-native ligands do not interfere with ferrocytochrome *c* refolding the very act of forming the native Fe^{2+}−M80 bond is critical in determining the speed of folding. Consider the folding picture in the absence of CO. In general, the entire polypeptide has to be configured to make way for the formation of

secondary structures and native tertiary contacts. The important interactions specific to achieving the native conformation of the M80 residue are the Fe^{2+}−M80 bond and the two key hydrogen-bonding interactions—one between the sulfur atom of M80, already engaged in iron bonding, and the side-chain oxygen of Y67, and the other between the main-chain nitrogen of M80 and the hydroxyl oxygen of T78. When the polypeptides are transferred to a strongly folding milieu, the affinity of the M80 ligand for the Fe^{2+} atom, relative to that of the other three non-native ligands, is expected to increase largely. Also, the dissociation times of the non-native ligands are likely to decrease by severalfold. These expectations together with the fact that a fraction of the unfolded chain ensemble is already M80-liganded, suggest that the Fe^{2+}−M80 bonding configuration appears at an early stage of folding. The two hydrogen bonds involving M80, Y67, and T78 are likely to form at a later stage following the acquisition of secondary structure, since the latter two residues are parts of the 60's helix (residues 60−69) and the β(II)-turn (residues 75−79), and experiments have suggested that secondary structures do not form in the early phase(s) of cytochrome *c* folding (*63*, *64*). The asynchrony in Fe^{2+}−M80 bonding and hydrogen bond formation is expected to produce two M80-related kinetic barriers. Relative magnitudes of the two barriers need to be determined. Carbonmonoxycytochrome *c*, by the virtue of possessing Fe^{2+}−CO bonding configuration, does not encounter the barriers, and hence folding is accelerated.

Unfolding. The effect of the native-state Fe^{2+}−M80 bonding on the unfolding rate of the protein is even more striking (Figure 6). At 10 °C, pH 7, ferrocytochrome *c* unfolds with a rate constant, $k_u(H_2O)$, of 6.3×10^{-16} s^{-1} (Table 3). It is remarkable that the rate is increased by more than 10 orders of magnitude to $\sim 4.6 \times 10^{-5}$ s^{-1} for carbonmonoxycytochrome *c*. The corresponding decrease in the activation energy barrier, E_a^u ($\sim$14.2 kcal mol^{-1}), strongly suggests that the rupture of the Fe^{2+}−M80 bond is the rate-limiting step in the unfolding of ferrocytochrome *c*. As already mentioned, the Fe^{2+}−M80 bond in native ferrocytochrome *c* is so strong that even CO fails to break it. Unfolding of ferrocytochrome *c* is slow, monoexponential, and simple (*13*). There is no burst-unfolding phase in stopped-flow kinetics monitored by tryptophan fluorescence or far-UV CD, implying the absence of submillisecond processes. In unfolding, the rates of dismantling of secondary and tertiary structures, water intrusion into the protein core, and possible swelling of the protein are all limited by breakage of the Fe^{2+}−M80 bond. The lone phase of ferrocytochrome *c* unfolding along with the observation of little structural unfolding concomitant with Fe^{2+}−M80 → Fe^{2+}−CO replacement under strongly native-like conditions indicates that the rupture of the Fe^{2+}−M80 bond must precede the main structural unfolding step. The native state of carbonmonoxycytochrome *c* could not exist if the event of Fe^{2+}−M80 rupture followed the structural unfolding step. The native structure of cytochrome *c* apparently does not unfold readily without first deligating M80, which presents the major kinetic barrier to unfolding. The limiting role of the iron−M80 bond has also been shown for the oxidized forms of horse cytochrome *c* (*67*) and *Rhodobacter capsulatus* cytochrome c_2 (*68*). This M80-associated barrier must offer kinetic stability to the protein. In the absence of the barrier, as it is in carbonmonoxycytochrome *c*, unfolding is extremely fast.

Importance of the Fe^{2+}−M80 Bond in the Maintenance of Cytochrome c Native Structure. The Fe^{2+}−M80 bond acts as the obligatory barrier in the folding of ferrocytochrome *c*, and indeed, the M80 residue is evolutionarily conserved (*69*). This residue is obviously indispensable for cytochorme *c* to function as an electron transfer protein. However, the molecule survives the replacement of M80 with extrinsic ligands. The replacement is achieved readily for ferricytochrome *c* at the cost of marginal loss of structure and stability. For example, native ferricytochrome *c* binds extrinsically added imidazole even under physiological conditions, and the transition midpoints (C_m) of denaturant-induced melting transitions in the presence and absence of imidazole are nearly identical (*24*, *70*). This study shows that such ligation-engineering in ferrocytochrome *c* requires some effort, and cannot be carried out directly, because the ferrous iron chemistry and a relatively more compact interior of the reduced protein (*71*, *72*) render extraordinary stability to the Fe^{2+}−M80 bond. The data presented in this paper also show large changes in the thermodynamic stability and folding and unfolding kinetics of the protein as a consequence of the Fe^{2+}−M80 → Fe^{2+}−CO replacement.

The thermodynamic and kinetic stability provided by the Fe^{2+}−M80 bond and the M80−associated hydrogen bonding interactions is advantageous for ferrocytochrome *c* to function as an electron donor to acceptors, including cytochrome b_5 and cytochrome *c* oxidase. In electron transfer, the intermolecular interactions between the donor and the acceptor molecule are electrostatic, and hence extensile in nature. This mode of intermolecular association facilitates rapid and often large-scale conformational fluctuations of the individual proteins in the complex in order to find the optimal heme−heme orientation favorable for electron transfer. Molecular dynamics studies of a cytochrome *c*−cytochrome b_5 electron transfer complex have actually shown that the molecular interaction is flexible and that many transient geometries of the complex appear (*73*). It is suggested that the high energy unfolding barrier due to the Fe^{2+}−M80 bond detected in this study provides sufficient kinetic stability to ferrocytochrome *c*, so that the protein is protected from unfolding during the high-frequency large-amplitude conformational fluctuations in the electron donor−acceptor complex.

ACKNOWLEDGMENT

The authors are grateful to Dr. S. Ramachandran and Ms. Asha of the Center for Cellular and Molecular Biology (CCMB) for extending instrumentation support. Earlier stopped-flow data were collected using the instrument in Jayant Udgaonkar's laboratory. The authors thank Professor D. Basavaiah for support and encouragement.

REFERENCES

1. Williams, S., Causgrove, T. P., Gilmanshin, R., Fang, K. S., Callender, R. H., Woodruff, W. H., and Dyer, R. B. (1996) *Biochemistry 35*, 691−697.
2. Lednev, I. K., Karnoup, A. S., Sparrow, M. C., and Asher, S. A. (1999) *J. Am. Chem. Soc. 121*, 8074−8086.
3. Thompson, P. A., Eaton, W. A., and Hofrichter, J. (1997) *Biochemistry 36*, 9200−9210.
4. Muñoz, V., Thompson, P. A., Hofrichter, J., and Eaton, W. A. (1997) *Nature 390*, 196−199.

5. Muñoz, V., Henry, E. R., Hofrichter, J., and Eaton, W. A. (1998) *Proc. Natl. Acad. Sci. U.S.A. 95*, 5872−5879.
6. Eaton, W. A., Muñoz, V., Thompson, P. A., Henry, E. R., and Hofrichter, J. (1998) *Acc. Chem. Res. 31*, 745−753.
7. Huang, G. S., and Oas, T. G. (1995) *Proc. Natl. Acad. Sci. U.S.A. 92*, 6878−6882.
8. Schindler, T., Herrler, M., Marahiel, M. A., and Schmid, F. X. (1995) *Nat. Struct. Biol. 2*, 663−673.
9. Villegas, V., Azuaga, A., Catasus, L. I., Reverter, D., Mateo, P. L., Aviles, F. X., and Serrano, L. (1995) *Biochemistry 34*, 15105−15110.
10. Pascher, T., Chesick, J. P., Winkler, J. R., and Gray, H. B. (1996) *Science 271*, 1558−1560.
11. Perl, D., Welker, C., Schindler, T., Schröder, K., Marahiel, M. A., Jaenicke, R., and Schmid, F. X. (1998) *Nat. Struct. Biol. 5*, 229−235.
12. Wildegger, G., Liemann, S., and Glockshuber, R. (1999) *Nat. Struct. Biol. 6*, 550−553.
13. Bhuyan, A. K., and Udgaonkar, J. B. (2001) *J. Mol. Biol. 312*, 1135−1160.
14. Jackson, S. E., and Fersht, A. R. (1991) *Biochemistry 30*, 10428−10435.
15. Viguera, A. R., Martinez, J. C., Filimonov, V. V., Mateo, P. L., and Serrano, L. (1994) *Biochemistry 33*, 2142−2150.
16. Van Nuland, N. A. J., Meijberg, W., Warner, J., Forge, V., Scheek, R. M., Robillard, G. T., and Dobson, C. M. (1998) *Biochemistry 37*, 622−637.
17. Otzen, D. E., Kristensen, O., Proctor, M., and Oliveberg, M. (1999) *Biochemistry 38*, 6499−6511.
18. Sosnick, T. R., Mayne, L., Hiller, R., and Englander, S. W. (1994) *Nat. Struct. Biol. 1*, 149−156.
19. Kiefhaber, T., and Schmid, F. X. (1992) *J. Mol. Biol. 224*, 231−240.
20. Mullins, L. S., Pace, C. N., and Raushel, F. M. (1993) *Biochemistry 32*, 6152−6156.
21. Schmid, F. X. (1995) *Curr. Biol. 5*, 993−994.
22. Bhuyan, A. K., and Udgaonkar, J. B. (1999) *Biochemistry 38*, 9158−9168.
23. Waldburger, C. D., Jonsson, T., and Sauer, R. T. (1996) *Proc. Natl. Acad. Sci. U.S.A. 93*, 2629−2634.
24. Elöve, G. A., Bhuyan, A. K., and Roder, H. (1994) *Biochemistry 33*, 6925−6935.
25. Muthukrishnan, K., and Nall, B. T. (1991) *Biochemistry 30*, 4706−4710.
26. Pierce, M. M., and Nall, B. T. (1997) *Protein Sci. 6*, 618−627.
27. Colón, W., Wakem, L. P., Sherman, F., and Roder, H. (1997) *Biochemistry 36*, 12535−12541.
28. Hanson, J. C., and Schoenborn, B. P. (1981) *J. Mol. Biol. 153*, 117−146.
29. Heidner, E. J., Ladner, R. C., and Perutz, M. F. (1976) *J. Mol. Biol. 104*, 707−722.
30. Santoro, M. M., and Bolen, D. W. (1988) *Biochemistry 27*, 8063−8068.
31. Silow, M., and Oliveberg, M. (1997) *Biochemsitry 36*, 7633−7637.
32. Banerjee, R. (1983) in *Brussels Hemoglobin Symposium* (Geroges Schnek, A., and Paul, C. Eds.), pp 123−135, Éditions de l′Université de Bruxelles, Brussels.
33. Onwubiko, H. A., Hazzard, J. H., Noble, R. W., and Caughey, W. S. (1982) *Biochem. Biophys. Res. Com. 106*, 223−228.
34. Choc, M. G., and Caughey, W. S. (1981) *J. Biol. Chem. 256*, 1831−1838.
35. Moon, R. B., and Richards, J. H. (1974) *Biochemistry 13*, 3437−3443.
36. Vanderkooi, J. M., and Erecinska, M. (1975) *Eur. J. Biochem. 60*, 199−20.
37. Tsong, T, Y. (1974)*J. Biol. Chem. 249*, 1988−1990.
38. Bushnell, G. W., Louie, G. V., and Brayer, G. D. (1990) *J. Mol. Biol. 214*, 585−595.
39. Matouschek, A., Kellis, J. T., Jr., Serrano, L., Bycroft, M., and Fersht, A. R. (1990) *Nature 346*, 440−445.
40. Kawahara, K., and Tanford, C. (1966) *J. Biol. Chem. 241*, 3228−3232.
41. Jacob, M., and Schmid, F. X. (1999) *Biochemistry 38*, 13773−13779.
42. Schejter, A., and Plotkin, B. (1988) *Biochem. J. 255*, 353−356.
43. George, P., and Schejter, A. (1964) *J. Biol. Chem. 239*, 1504−1508.
44. Schejter, A., and Aviram, I. (1970) *J. Biol. Chem. 245*, 1552−1557.
45. Wüthrich, K., Aviram, I., and Schejter, A. (1971) *Biochim. Biophys. Acta 253*, 98−103.
46. Brunori, M., Wilson, M. T., and Antonini, E. (1972) *J. Biol. Chem. 247*, 6076−6081.
47. Wilson, M. T., Brunori, M., Rotilio, G. C., and Antonini, E. (1973) *J. Biol. Chem. 248*, 8162−8169.
48. Alberding, N., Austin, R. H., Chan, S. S., Eisenstein, L., Frauenfelder, H., Good, D., Kaufmann, K., Marden, M., Nordlund, T. M., Reinisch, L., Reynolds, A. H., Sorensen, L. B., Wagner, G. C., and Yue, K. T. (1978) *Biophys. J. 24*, 319−334.
49. Theorell, H., and Åkesson, A. (1941) *J. Am. Chem. Soc. 63*, 1812−1827.
50. Jones, C. M., Henry, E. R., Hu, Y., Chan, C. K., Luck, S., Bhuyan, A., Roder, H., Hofrichter, J., and Eaton, W. A. (1993) *Proc. Natl. Acad. Sci. U.S.A. 90*, 11860−11864.
51. Bhuyan, A. K., and Udgaonkar, J. B. (1998) *Proteins: Struct. Funct. Genet. 32*, 241−247.
52. Xu, Y., Mayne, L. C., and Englander, S. W. (1998) *Nat. Struct. Biol. 5*, 774−778.
53. Mayne, L., and Englander, S. W. (2000) *Protein Sci. 9*, 1873−1877.
54. Shortle, D., Stites, W. E., and Meeker, A. K. (1990) *Biochemistry 29*, 8033−8041.
55. Dill, K. A., and Shortle, D. (1991) *Annu. Rev. Biochem. 60*, 795−825.
56. Ascenzi, P., Coletta, M., Santucci, R., Polizio, F., and Desideri, A. (1994) *J. Inorg. Biochem. 53*, 273−280.
57. Roder, H., and Colón, W. (1997) *Curr. Opin. Struct. Biol. 7*, 15−28.
58. Shastry, M. C. R., and Roder, H. (1998) *Nat. Struct. Biol. 5*, 385−392.
59. Qi, P. Q., Sosnick, T. R., and Englander, S. W. (1998) *Nat. Struct. Biol. 5*, 882−884.
60. Sosnick, T. R., Mayne, L., and Englander, S. W. (1996) *Proteins 24*, 413−426.
61. Sosnick, T. R., Shtilerman, M. D., Mayne, L., and Englander, S. W. (1997) *Proc. Natl. Acad. Sci. U.S.A. 94*, 8545−8550.
62. Bhuyan, A. K., and Udgaonkar, J. B. (1999) in *Perspectives in Structural Biology* (Vijayan, M., et al., Eds.), pp 293−303, University Press (India) Limited, Hyderabad, India.
63. Akiyama, S., Takahashi, S., Ishimori, K., and Morishima, I. (2000) *Nat. Struct. Biol. 7*, 514−520.
64. Chen, E., Wittung-Stafshede, P., and Kliger, D. S. (1999) *J. Am. Chem. Soc. 121*, 3811−3817.
65. Pierce, M. M., and Nall, B. T. (2000) *J. Mol. Biol. 298*, 955−969.
66. Zwanzig, R. W. (1997) *Proc. Natl. Acad. Sci. U.S.A. 94*, 148−150.
67. Colón, W., Elöve, G. A., Wakem, L. P., Sherman, F., and Roder, H. (1996) *Biochemistry 35*, 5538−5549.
68. Sauder, J. M., MacKenzie, N. E., and Roder, H. (1996) *Biochemistry 35*, 16852−16862.
69. Dickerson, R. E. (1972) *Sci. Am. 226*, 58−70.
70. Chan, C.-K., Hu, Y., Takahashi, S., Rousseau, D. L., Eaton, W. A., and Hofrichter, J. (1997) *Proc. Natl. Acad. Sci. U.S.A. 94*, 1779−1784.
71. Takano, T., and Dickerson, R. E. (1981b) *J. Mol. Biol. 153*, 95−115.
72. Berghuis, A. M., and Brayer, G. D. (1992) *J. Mol. Biol. 223*, 959−976.
73. Wendoloski, J. J., Matthew, J. B., Weber, P. C., and Salemme, F. R. (1987) *Science 238*, 719−866.
74. Mims, M. P., Porras, A., Olson, J. S., Peterson, J., and Noble, R. W. (1983) *J. Biol. Chem. 258*, 14229−14232.

BI0204443